Bulletin of the Seismological Society of America, Vol. 70, No. 4, pp. 963–983, August 1980

TELESEISMIC OBSERVATIONS OF THE 1976 FRIULI, ITALY EARTHQUAKE SEQUENCE

By John Cipar

ABSTRACT

Teleseismic long-period body and surface waves radiated by the May 6, 1976 Friuli, Italy earthquake and its principal aftershock of September 15, 1976 (09h 21m) are studied to determine source characteristics. Focal mechanisms along with geological evidence suggest that both events represent the underthrusting of the Friuli Plain beneath the southern Alps. The depths of both earthquakes, estimated by matching synthetic body-wave seismograms to observations, are found to lie between 6 and 10 km. It is not possible to discern any evidence of source directivity in the observed main shock body waves. Synthetic seismogram calculations which include rupture effects suggest that the fault length of the main shock could not be much larger than 16 km for a unilaterally propagating fault or about 24 km for a symmetrical rupture assuming a rupture velocity of 3.0 km/sec. Observations of 100-sec Rayleigh waves confirm the focal mechanism deduced from body waves, but suggest that the seismic moment of the main shock is 5×10^{25} dyne-cm compared to 2.9×10^{25} dyne-cm estimated from body waves. The *P*-wave moment of the aftershock is 1×10^{25} dyne-cm. The aftershock studied in this paper is one of four large events which occurred in the epicentral area of the main shock more than 4 months after the main shock. These aftershocks had a combined seismic moment over twice that of the main shock. It is suggested that these earthquakes represent deformation in a different part of the seismic zone than the main shock. Large earthquakes with series of severe aftershocks are well known in the historical record of the Friuli region. The average displacement and stress drop are estimated to be 33 cm and 12 bars for the main shock and 33 cm and 24 bars for the aftershock.

Introduction

One of the most damaging earthquakes in the European area in recent years struck the Friuli region of northeastern Italy on May 6, 1976. The main shock caused heavy loss of life and a great amount of property damage and was followed by an aftershock sequence of unusual severity.

The seismograms written by the Friuli earthquake and its aftershocks present an opportunity to understand the dynamics of faulting in a continental environment. The main shock and several aftershocks were well recorded teleseismically. Moreover, accelerograms were obtained for the main shock and aftershocks from stations in the epicentral area. This data set provides an opportunity to view the earthquakes in four spectral bands: long-period surface waves, long- and short-period teleseismic body waves, and near-field ground displacement. In addition, the large magnitude of several of the aftershocks relative to the main shock is a feature of this earthquake sequence that is not commonly observed in other seismic zones. From a tectonic point of view, knowledge of the mechanism of the earthquake is important in elucidating the mechanics of the collision of Africa and Eurasia.

This paper discusses various features of the source properties of the main shock and aftershock of September 15, 1976 (09h 21m) which can be inferred from teleseismic long-period body- and surface-wave data. Fault mechanism, source depth, and nature of fault rupture can be deduced from body waves. Additional data on the long-period nature of the source is available from surface waves. Finally, the

long-term pattern of seismic strain release in the region is revealed by the aftershock sequence.

Tectonic Setting

The Friuli-Venetia-Giulia region of northeastern Italy extends from Austria on the north to the Adriatic Sea on the south and is bordered on the east by Yugoslavia. The region can be divided into several distinct topographic elements (Martinis, 1975). Along the Austrian border are the Carnic Alps, composed principally of Paleozoic rocks. South of the Carnic Alps are the largely Mesozoic Tolmezzo Alps in the western part of the area and the Julian Alps in the east. South of the latitude of the Tagliamento River, the mountains become lower in elevation. These ranges known as the Pre-Alps, are underlain by Cenozoic flysch and molasse deposits. Between the Pre-Alps and the Adriatic Sea is the extensive Friuli Plain of Quaternary sediments. To the east, in Yugoslavia, the Dinaric Alps trend southeastward down the Balkan Peninsula.

The Carnic, Tolmezzo, and Julian Alps, together with the Pre-Alps, constitute the southern Alps in a geological sense (Angenheister *et al.*, 1972). The southern Alps are separated from the eastern Alps by an important structural boundary(Figure 1), the Periadriatic Line, which forms the northern boundary of the Carnic Alps (Angenheister *et al.*, 1972; Martinis, 1975). In general, the southern Alps have suffered less metamorphism and tectonism than the rocks north of the Periadriatic Line (Angenheister *et al.*, 1972). In the Friuli region, the structural grain changes from northwest-southeast Dinaride trends near the border with Yugoslavia, to more east-west trending structures of the Southern Alps in the west.

Throughout much of the Mesozoic period, shallow-water deposition of calcareous rocks occurred through the Friuli region (Martinis, 1975), although the presence of deep basins is indicated by pelagic sedimentation. Beginning in early Cenozoic times, the tectonic environment became more unstable. Eocene flysch deposits, which now outcrop at the edge of the Friuli Plain, mark the beginning of the Alpine orogeny which culminated in the Upper Miocene and Pliocene periods (Amato *et al.*, 1976). Subaerial depositional environment has prevailed over the Friuli region from the Oligocene to the present.

The most important structural feature in the epicentral area is the so-called "Periadriatic Thrust" (Amato *et al.*, 1976; Martinis, 1975) which is a complex zone of northward dipping thrust faults (Figure 1). The Periadriatic Thrust is not to be confused with the Periadriatic Line (heavy dashed line in Figure 1) mentioned above which structurally separates the Eastern and Southern Alps. In addition to the mapped faults which outcrop, a number of similar structures have been found in the subsurface of the Friuli Plain on seismic reflection profiles (Amato *et al.*, 1976).

In a larger context, McKenzie (1972) suggests that the Adriatic Sea and the coastal areas of Italy and Yugoslavia form a tongue of the African plate which is underthrusting Eurasia in northeastern Italy and Yugoslavia. The African-Eurasian plate boundary is inferred from seismicity (Papazachos, 1973) to extend from Tunisia, through Sicily and the toe of Italy, up the Italian peninsula, across the southern Alps and down the coast of Yugoslavia (Figure 1). Lort (1971) on the other hand, suggests that the Adriatic Sea is a separate microplate, the Apulian plate which may move independently of the larger plates. Except for the existence of a plate boundary across the mouth of the Adriatic Sea, the interpretations of Lort and McKenzie are similar. In both cases, compressional tectonics would be expected in northeastern Italy and adjacent Yugoslavia.

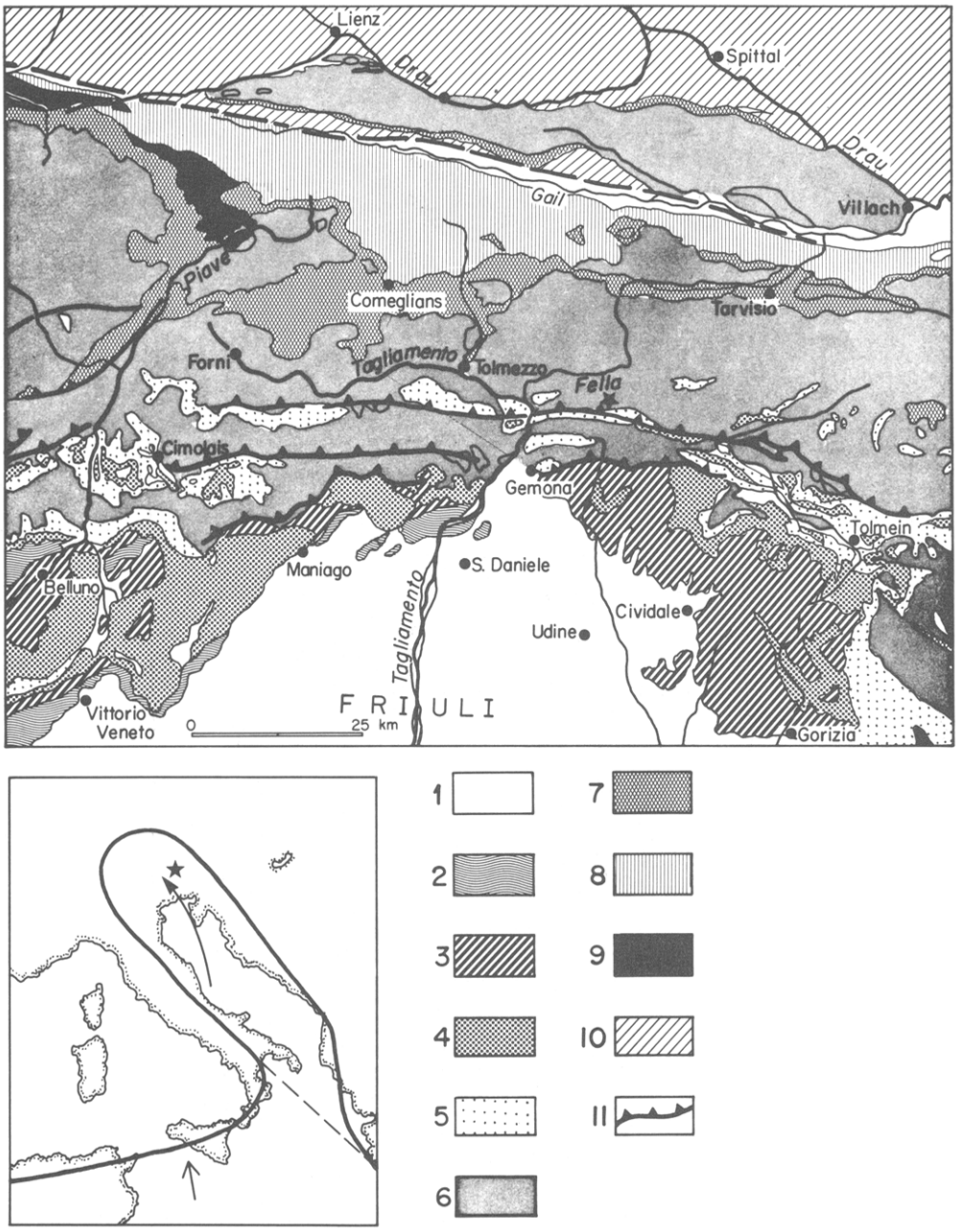

FIG. 1. Geological and plate tectonic setting of the Friuli earthquake sequence. The *upper* figure shows the geology after Gwinner (1971). The star near the center of the figure shows the ISC location of the main shock. The heavy dashed line along the Gail River is the Periadriatic Line (see text). Geological units are: (1) Quaternary, (2) Miocene molasse, (3) Eocene-Oligocene flysch, (4) Cretaceous carbonate, (5) Jurassic undivided, (6) middle and upper Triassic, (7) Triassic and Permian, (8) Paleozoic of the Carnic Alps, (9) quartz phyllite, (10) crystalline rocks of the eastern Alps, and (11) thrust fault. The *lower* figure shows the plate tectonic interpretation of McKenzie (1972) and Lort (1971). The dashed line represents the inferred southwestern boundary of the Apulian plate. Arrows indicate direction of plate motion. Star is location of main shock.

SEISMICITY

Northern Italy, including the Friuli region, was characterized as an area of low-to-moderate seismicity by Gutenberg and Richter (1954), although Karnik (1971, p. 184) was impressed with the activity in the Friuli region. Reports of historical

earthquakes before 1900 have been collected by Ambraseys (1976a) and Karnik (1971). The most notable earthquakes were the shocks of 1348 and 1511. While the amount of damage due to these shocks was severe, both authors believe that none of the events exceeded magnitude $6\frac{3}{4}$. The severe damage caused by earthquakes in this region is due not so much to the large magnitude of the events but more because of poor construction techniques (Ambraseys, 1976a). The seismic activity of Friuli can be characterized by the occurrence of infrequent moderate earthquakes ($M_S <$ 7) separated by long quiescent periods, with only minor seismicity.

According to Ambraseys (1976a), there have been only two earthquakes since 1900 with surface-wave magnitude greater than 5.0 prior to the 1976 events (Table 1). An $m_b = 4.2$ (USGS) shock occurred on March 24, 1975 and was followed by a series of shocks which were felt in the Tolmezzo region through April 25 (ISC reports). The ISC does not report any further events in the epicentral area until the foreshock of the Friuli earthquake on May 6, 1976.

TABLE 1

SIGNIFICANT EARTHQUAKES IN THE FRIULI REGION

No.	Year	Date	Time	Lat. (°N)	Long. (°E)	Depth	m_b	M_s	References
	1348	Jan. 25		46.5	13.4				Ambraseys (1976)
	1511	Mar. 26		46.2	13.6				Ambraseys (1976)
	1928	Mar. 27	08h 32m	46.41	13.08	25		5.8	Ambraseys (1976)
	1936	Oct. 18	03h 10m	46.04	12.40	15		5.7	Ambraseys (1976)
	1975	Mar. 24	02h 33m	46.29	13.13	21			NEIS
0	1976	May 6	19h 59m	46.201	13.262	33N	4.5		NEIS
1	1976	May 6	20h 00m	46.36	13.28	9	6.0	6.5	NEIS
13	1976	May 11	22h 44m	46.27	12.99	11	5.2		NEIS
36	1976	Sept. 11	16h 31m	46.28	13.16	16	5.2	5.5	NEIS
37	1976	Sept. 11	16h 35m	46.30	13.20	20	5.3	5.4	NEIS
42	1976	Sept. 15	03h 15m	46.30	13.20	10G	5.7	6.0	NEIS
46	1976	Sept. 15	09h 21m	46.32	13.13	17	5.4	5.9	NEIS
	1977	Sept. 16	23h 48m	46.27	12.97	25	5.1	5.1	NEIS

The main shock (May 6, 1976, 20h 00m) was preceded by an $M_L = 4.5$ foreshock at 19h 59m and followed by numerous aftershocks which decreased in magnitude and frequency until September 1976. The normal decay of the aftershock sequence was shattered by two pairs of strong earthquakes on September 11 (16h 31m and 16h 35m) and September 15 (03h 15m and 09h 21m). Seismic activity declined markedly after these earthquakes, although a magnitude 5.1 shock occurred 1 yr later in September 1977.

Unfortunately, there is some ambiguity concerning the location on the epicenter of the main shock relative to the aftershock distribution. Table 2 gives the hypocenter determinations of various agencies which are shown as stars on Figure 3. The ISC locations of the larger aftershocks are shown in Figure 2. While there is activity over a broad area, most aftershocks are concentrated within a roughly elliptically shaped region 30-km long by 18-km wide. Referring to Figure 3, note that most of the agencies place the main shock near the eastern edge of the aftershock distribution (outlined by the dashed line), except Rome, which puts the epicenter in the center of the distribution. To see if there are any systematic differences between Rome and ISC locations, the positions of several of the larger and presumably better located aftershocks as reported by each group are plotted in Figure 3. The arrows point from the ISC location to the Rome location. There seems to be no consistent shift of epicenters determined by one agency to the epicenters computed by the other.

To help resolve these discrepancies in locations, the main shock and two aftershocks were relocated relative to a third aftershock. Note that the Rome and ISC epicenters of event 36 (September 11, 16h 31m) are quite close. This event was large and well recorded and was chosen as the master event. Using the relative location

TABLE 2

MAIN SHOCK HYPOCENTER DETERMINATIONS, MAY 6, 1976

Agency*	Time (h m s)	Lat. (°N)	Long. (°E)	Depth	m_b	M_S	M_L
NEIS	20 00 11.6	46.356	13.275	9	6.0	6.5	
ISC	12.5	46.35	13.26	12	5.9		
Rome 1	12.2	46.15	13.11	26			6.2
Rome 2	8.6	46.29	13.13			Mag = 6.4	
CSEM	14.7	46.31	13.31	10			
C. & G. 1	11.278	46.253	13.240	8.19			
C. & G. 2	12.585	46.250	13.231	9.995			

* NEIS, National Earthquake Information Service, Preliminary Determination of Epicenters, Monthly Listing; ISC, International Seismological Centre, Edinburgh, Scotland; Rome, Instituto Nazionale di Geofisica, Rome; CSEM, Centre Seismologique Europeo-Mediterranean; C. & G., Console and Gasparini (1976).

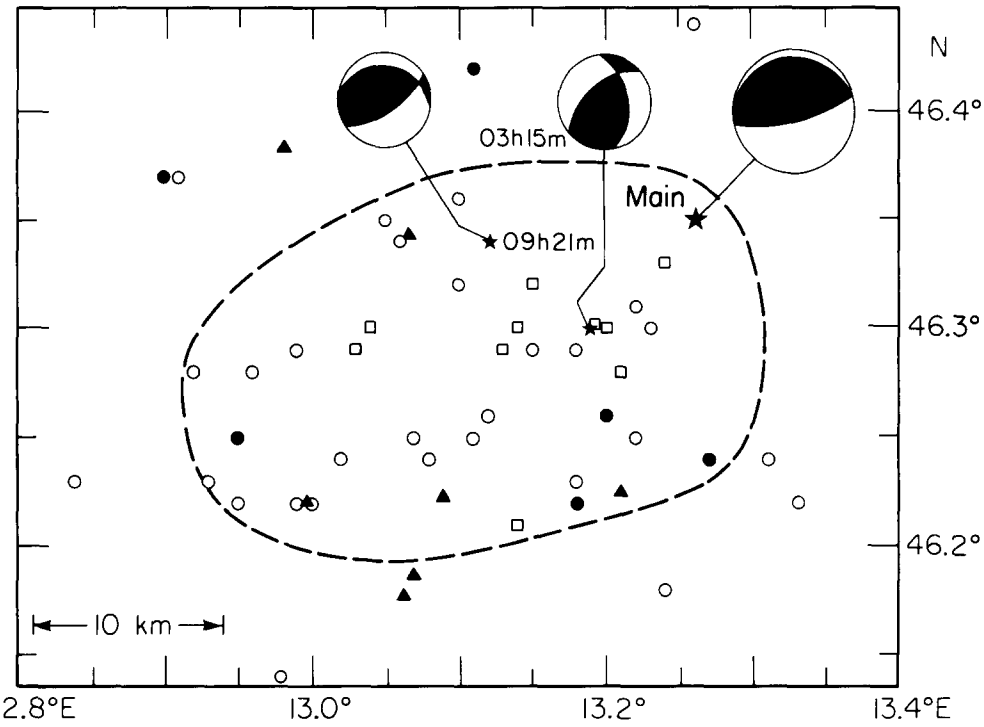

FIG. 2. Epicenters of the main shock and larger aftershocks of the Friuli earthquake sequence as reported by the ISC. Large star indicates the main shock. Closed circles represent aftershocks which occurred within the first 24 hr, and open circles are later aftershocks up to September 11. Smaller stars are epicenters of the two largest earthquakes on September 15. Open squares are aftershocks of these events. Focal mechanisms are determined in this paper with compressional quadrants shaded. Heavy dashed line denotes the approximate limit of aftershock concentration. Triangles are accelerograph stations.

method implemented by Chung and Kanamori (1976), the locations of the main shock and aftershocks 46 and 13 relative to aftershock 36 were computed (shown as filled squares in Figure 3). There seems to be no gross errors in the method since in both cases, the relative location of the aftershocks are in the vicinity of the absolute

locations determined both by Rome and ISC. The relative location places the main shock on the eastern edge of the aftershock distribution nearer to the ISC location than to the epicenter of Rome.

There are several other points to be made about the aftershock distribution. First, the larger, first day aftershocks (shown as closed circles in Figure 2) occur along the margins of the aftershock zone. Second, the September earthquakes (open squares in Figure 2) occur within the aftershock zone of the main event. These observations are in agreement with the conclusions of a more complete study of aftershock locations by Cagnetti and Console (1977) who also show that the location of activity shifts during the course of the aftershock sequence. In a later section, the temporal pattern of energy release during the aftershock sequence will be examined.

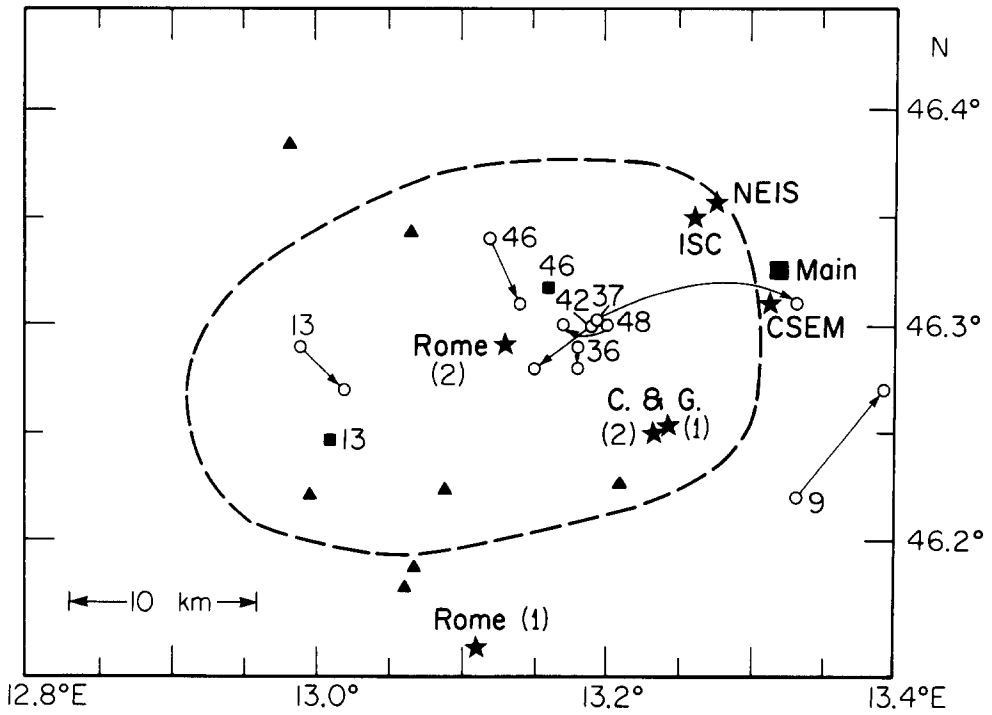

FIG. 3. Locations of the main shock and largest aftershocks. Main shock epicenters determined by various agencies are indicated by stars (Table 2). Aftershock epicenters (numbers correspond to Table 1) calculated by ISC and Rome are indicated by open circles; arrows point from ISC location to Rome location. Filled squares indicate locations of main shock and aftershocks 13 and 46 relative to aftershock 36 determined in this paper.

BODY WAVE DATA

Many of the results of this paper are obtained by matching synthetic seismograms to observed records. To create synthetic seismograms, the response of a layered medium is convolved with operators describing source time history, attenuation, and instrument response. The medium response can be computed using either generalized rays (Helmberger, 1974; Langston and Helmberger, 1975) or layer matrices (Haskell, 1962). At distances closer than about 30°, upper-mantle structures create arrivals on seismograms which are not associated directly with the source properties of the earthquake. At distances greater than 85°, core effects begin to influence records. Thus, the distance window for *P*-wave observations is 30° to 85° and 45° to 80° for *S* waves. Within these distance ranges, the effect of the mantle on

the records is mainly due to anelastic attenuation and geometrical spreading. Futterman's (1962) Q-operator was used to construct the attenuation operator. Initially, $T/Q = 1.0$ sec for P waves and $T/Q = 4.0$ sec for S waves was used. Other values of T/Q were tried because of the uncertainty of the S-wave attenuation; the results of these experiments are described later.

The main shock on May 6, 1976 and the aftershock of September 15, 1976 were, at best, moderate-sized earthquakes but nonetheless were well recorded by WWSSN stations around the world. Stations to be used for the body- and surface-wave analysis were chosen based on clarity of recording and absence of long-period noise. Station information is listed in Table 3. Relevant portions of the seismograms were

TABLE 3
Station Data

Station	Delta (deg.)	Azimuth (deg.)	Back Azimuth (deg.)
AAE	43.1	141.5	334.2
ALQ	82.5	314.0	37.3
ANP	83.7	59.8	318.7
BEC	59.6	286.4	51.7
BLA	66.5	299.8	48.8
BOG	84.9	271.5	44.0
BUL	67.6	164.4	348.6
CAR	75.7	270.4	44.7
CHG	73.7	79.6	314.1
COR	81.6	330.3	28.7
COL	68.1	351.4	14.0
DAV	99.9	68.6	319.5
DUG	81.3	321.3	34.4
GOL	78.3	316.4	38.3
HKC	81.3	66.8	316.6
KTG	29.6	336.8	125.9
LON	79.3	330.5	29.8
LPB	96.0	252.7	43.6
MAT	83.8	41.5	325.3
MSH	35.7	89.4	301.0
MSO	76.3	325.8	34.5
NAT	51.8	149.4	339.4
PRE	73.0	165.9	349.2
QUE	44.3	91.9	307.0
SHA	75.6	299.5	44.4
SHI	34.7	104.7	309.8
SNG	83.0	86.8	315.9
WES	57.8	299.4	54.5

digitized on an electronic digitizing table and then detrended and interpolated by computer. P and S waves were corrected for instrumental magnification and plotted at uniform time scale. East-west and north-south components of the S waves were rotated to obtain pure SH and SV records.

Long-Period Body Waves

The first step in computing synthetic body-wave seismograms is to prepare a focal mechanism solution. P-wave first motions were read on long-period vertical seismographs of the WWSSN and other stations. For the main shock (Figure 4), the available data define the steeply dipping nodal plane quite well, while the other plane is almost completely unconstrained.

In cases in which the orientation of one nodal plane is ambiguous, S waves can often be used to fix the location of the unknown plane. The technique of S-wave polarization is well known (Müller, 1977). In this paper, SV and SH synthetic seismograms will be computed for various trial orientations and compared to the observed records. The trial mechanism which gives the most consistent fits is inferred to be the correct focal mechanism. This procedure is really an extension of the polarization method in that the whole waveform and not just certain amplitude measurements are used.

Because factors such as source depth and duration, in addition to focal mechanism, influence the waveforms of S, it is necessary to have some estimates of these quantities before determining the mechanism. Fortunately, the focal mechanism and station distribution for the main shock allow us to pick stations at which the P wave is not particularly sensitive to the orientation of the shallowly dipping (and originally unknown) nodal plane. By examining the focal mechanism on Figure 7, it

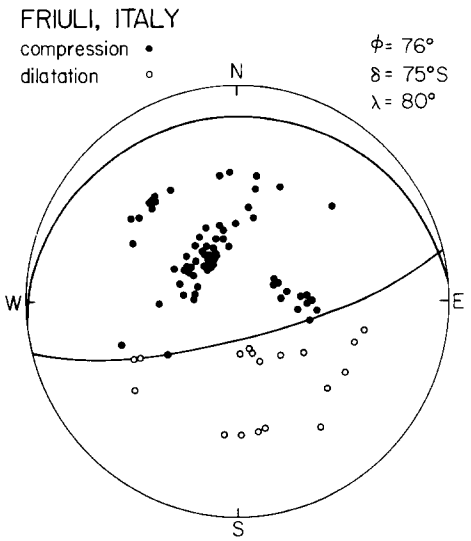

FIG. 4. P-wave focal mechanism of main shock of May 6, 1976. Data read on WWSSN long-period vertical seismographs and on other long-period stations in Europe and plotted on lower half of focal sphere. Shallowly dipping plane is constrained by S-wave data.

can be seen that stations such as MSO, BLA, and HKC will always be near the maximum of the P-wave radiation pattern for any possible orientation of the shallowly dipping plane. Calculating synthetic P waves for various depth and time function combinations (an example is shown in Figure 5) shows that the observed records are best fit with a 4.5-sec trapezoidal time function at a source depth of 8 to 10 km.

With the source depth, time function, and orientation of one nodal plane known, S waves can be used to determine the position of the second nodal plane in the manner described above. Figure 6 shows representative SH and SV waves for various rake angles corresponding to different orientations of the shallowly dipping nodal plane; the steep plane is fixed at strike = 76° and dip = 75°S. The best agreement is for a rake of about 80°, corresponding to a plane striking 86° and dipping 15°N.

Console (1976), Ebblin (1976), and Müller (1977) have also published mechanisms for the main shock. In each mechanism, the position of the steep, southeast dipping

plane is in good agreement with the results of this study. Müller used *S*-wave polarization techniques to determine the orientation of the second plane which he finds dips shallowly to the northwest. In Ebblin's mechanism, the second plane dips shallowly west-northwest, constrained by a single nearby station. In contrast, the results of this paper indicate that the fault plane dips almost due north at a very shallow angle.

After the mechanism and depth of the earthquake have been determined, the next step is to include the effect of crustal structure in the synthetic waveforms. Angenheister *et al.* (1972) have published a north-south velocity profile for the southern Alps based on nearby refraction lines. Their structure has an upper crustal velocity of 6.0 km/sec extending to about 23 km interrupted by a low-velocity layer from 12 to 20 km. This low-velocity zone is quite prominent near the Alpine axis, but rather weak in the Friuli region. Below 23 km, the velocity increases to 6.8 km/sec at 30 km, to 7.0 km/sec at 36 km, and finally 8.0 km/sec at about 44 km. A

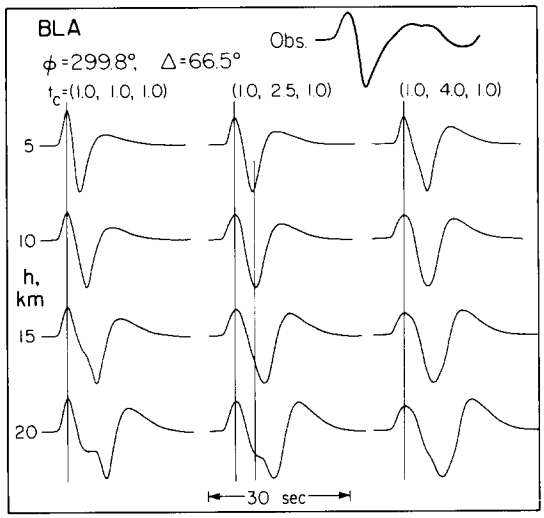

FIG. 5. Examples of synthetic waveforms computed for several combinations of source depth (h) and time function (t_c).

model based on an unreversed refraction profile through the epicentral area has been published by Finetti and Morelli (1972). Their model has an upper crustal velocity of 5.85 km/sec to 12.4 km, below which 6.2 km/sec material extends to 28 km. The lower crust has a velocity of 7.0 km/sec. Mantle velocity of 8.0 km/sec is reached at 45 km. In most important respects, this model is similar to the model of Angenheister *et al.* (1972). In particular, the presence of rather high velocity (7.0 km/sec) material just above the moho in both models is required to reduce strong phases reflected between the moho and the free surface which are then radiated to teleseismic distances. These phases arise on synthetic records when there is too large a velocity contrast across the moho; they are not observed on the real seismograms. The Angenheister *et al.* (1972) model was divided into discrete layers for use in the synthetic seismogram program and the low-velocity zone (which is not very pronounced in the Friuli region) was eliminated. *S*-wave velocities were calculated from the *P*-wave velocities by assuming a Poisson's ratio of 0.25. The resulting model is given in Table 4.

The matrix method of Haskell (1962) was used to compute the response of the layered crust to an embedded point source. By convolving the crustal response with a Q-operator, far-field source time history, and instrument response, realistic synthetic seismograms are created which can be compared directly to the observed records.

Figure 7 shows the observed records (heavy lines) and synthetics (light lines) computed for a source at 8-km depth in the Angenheister *et al.* (1972) structure.

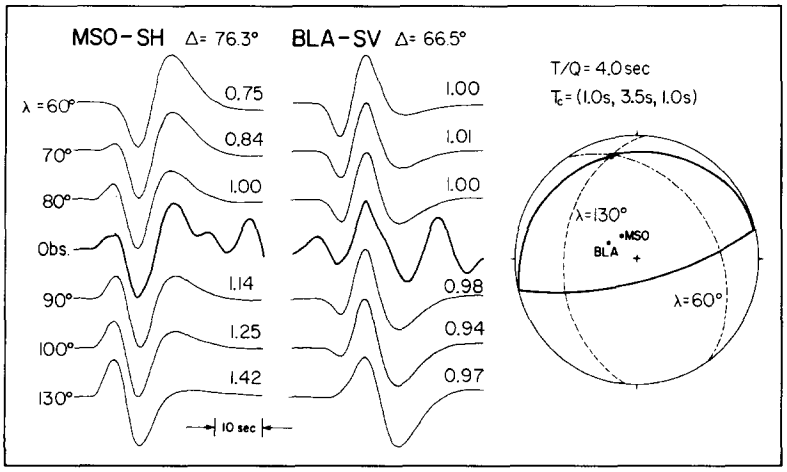

FIG. 6. Determination of shallowly dipping nodal plane using S-wave data. Note variation of SH-wave synthetics at MSO and SV-wave synthetics at BLA with change in rake angle. Best estimate is that the rake angle lies between 80° and 90°, corresponding to almost pure dip-slip fault mechanism.

TABLE 4

CRUSTAL MODEL (AFTER ANGENHEISTER ET AL., 1972)

Layer	P-Wave Velocity (km/sec)	S-Wave Velocity (km/sec)	Density (gr/cc)	Thickness (km)	Depth (km)
1	6.0	3.47	2.60	22.0	0.0
2	6.2	3.58	2.66	2.4	22.0
3	6.4	3.70	2.72	1.2	24.4
4	6.6	3.81	2.78	2.4	25.6
5	6.8	3.93	2.84	6.0	28.0
6	7.0	4.05	2.90	8.0	34.0
7	8.0	4.62	3.20	—	42.0

The overall agreement between synthetic and observed records is quite good, indicating that the basic parameters of the model are reasonable. Rather significant discrepancies occur for stations near nodal lines (AAE, BUL, and SHI) and for most stations after the first 15 sec. Nodal stations are especially sensitive to radiation pattern, and undoubtedly some of these discrepancies are due to the simple-point source model used to compute the synthetics. It is easy to imagine irregular fault propagation with the fault orientation changing as the rupture proceeds. In addition, the real Earth is certainly not as simple as the structure used, nor have any effects of the crust at the receiving station been taken into account.

S-wave data has already been used to constrain the focal mechanism. Figure 8 shows the observed synthetic SH and SV waves for the main shock. The synthetics have been computed for the same model used for the P-waves except that the length of the time function has been increased to 5.5 sec to better match the observed S-

wave duration. The overall fit between observed S-waves and synthetic records is good indicating that the source model is reasonable. With the exception of the SH wave at PRE (Figure 8), which is on a nodal line, the seismic moments calculated from the SH data are somewhat low compared to the P-wave moments. The above calculations were done assuming $T/Q = 4.0$ sec. Burdick and Mellman (1976) have suggested that T/Q for S waves should be 5.3 sec from the study of the Borrego Mountain, California earthquake. S-wave synthetics for the model with $T/Q = 5.3$ sec and $t_c = 4.5$ sec (the P-wave value) are almost indistinguishable from the model presented in Figure 8 ($T/Q = 4.0$, $t_c = 5.5$), except that the SH moments for the $T/Q = 5.3$-sec model are in somewhat better agreement with the P-wave moments.

The interpretation of the body-wave seismograms of the aftershock of September 15, 1976 at 09h 21m proceeds in the same manner as for the main shock. Like the main shock, the orientation of the steeply dipping plane of the aftershock was fixed

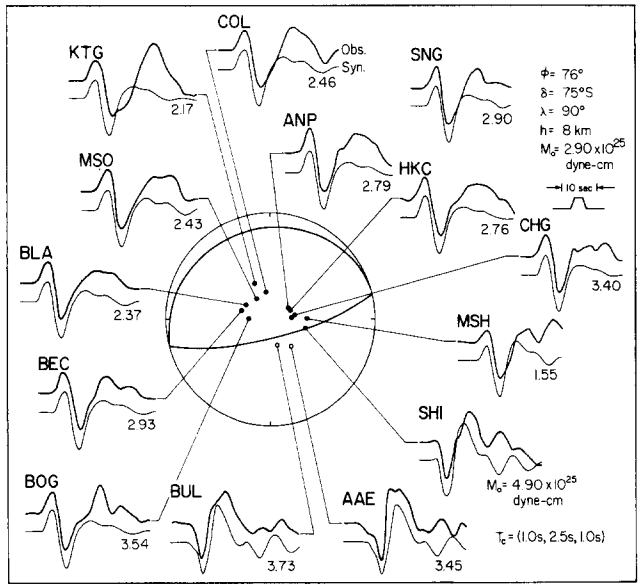

FIG. 7. Observed P waves (dark line) for main shock compared to synthetics (light line) computed for a point source at 8-km depth within the structure given in Table 4. Strike (ϕ), dip (δ), rake (λ), depth (h), average moment (M_0), and time function (t_c) are indicated.

by P-wave observations and the orthogonal plane was determined from S waves. The mechanism is shown in Figure 9. The strike and dip of the steep plane are 56° and 67°S, respectively. The shallowly dipping plane shown in Figure 9 corresponds to a rake of 70°. Observed and synthetic P and S waves are compared in Figures 10 and 11. The mechanisms of the main shock and aftershocks are similar, as are the depths, around 8 km. The far-field time function of the aftershock has a duration of 3 to 3.5 sec whereas the main shock is about 4.5-sec duration. The aftershock P-wave moment is 1.0×10^{25} dyne-cm compared to 2.9×10^{25} dyne-cm for the main shock.

The regional tectonics, in particular the mapped east-west striking thrust faults (Figure 1), suggest that for both the main shock and aftershock, the shallow, northward dipping nodal plane is the fault plane. In the case of the main shock, the roughly elliptically shaped aftershock distribution (Figure 2) also suggests that the shallowly dipping nodal plane is the fault plane (Cagnetti and Console, 1977). In this

case, the fault motion is nearly pure dip-slip with the northern block (Alps) overthrusting the sedimentary basin. The shallowly dipping plane of the 09h 21m aftershock mechanism is similar in orientation to that of the main shock, but the slip vector is more oblique.

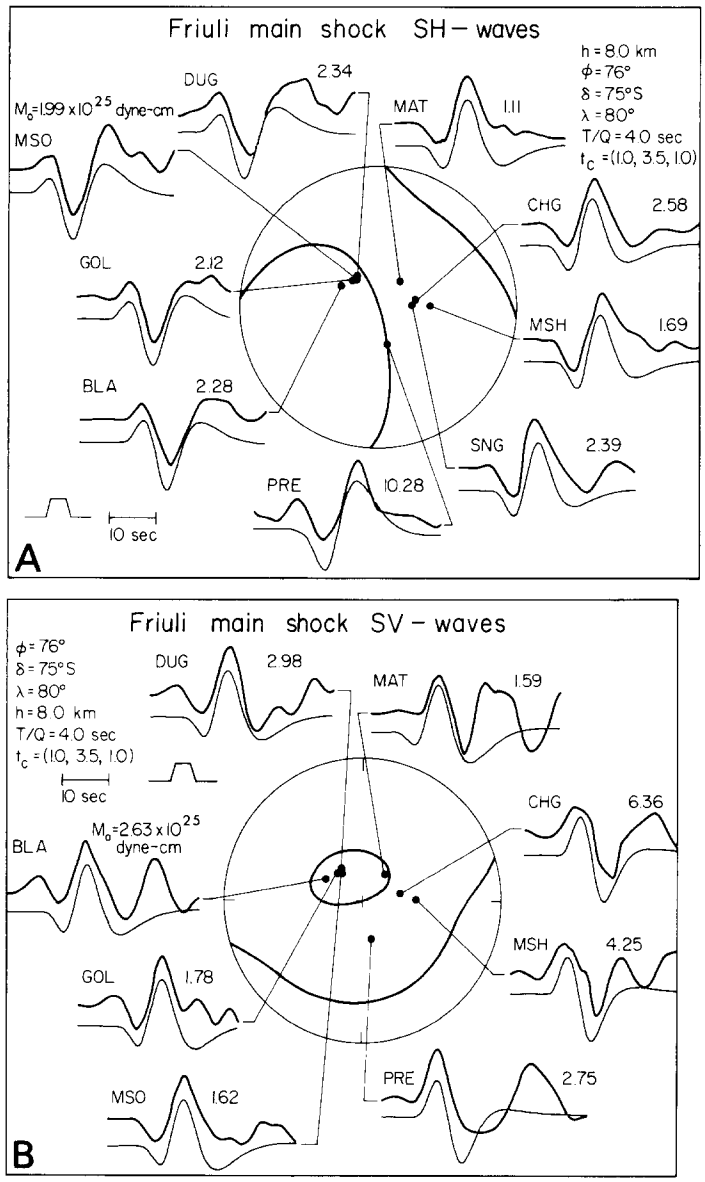

FIG. 8. *SH* and *SV* waves recorded from the Friuli earthquake compared to synthetics computed for a point source within a half-space. Attenuation is controlled by the ratio T/Q which is 4.0 sec for this case; time function is 5.5-sec duration. Other notation same as Figure 7.

A focal mechanism has also been prepared for the large aftershock which occurred at 03h 15m on September 15 (Figure 9). The *P* waves are small to begin with and because they are somewhat obscured by noise from a previous event, good first-motion readings are rare. Nevertheless, it is clear that the mechanism of this earthquake is somewhat different than the others studied in this paper. Certain

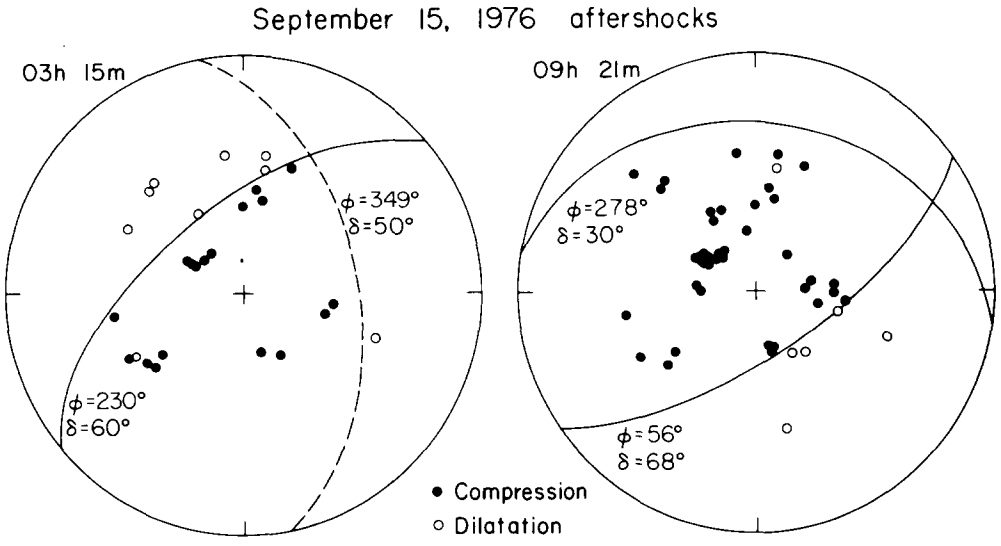

FIG. 9. *P*-wave nodal diagram for September 15, 1976 aftershocks at 03h 15m and 09h 21m. Data read from WWSSN long-period vertical records along with some auxiliary stations and plotted on lower half of focal sphere.

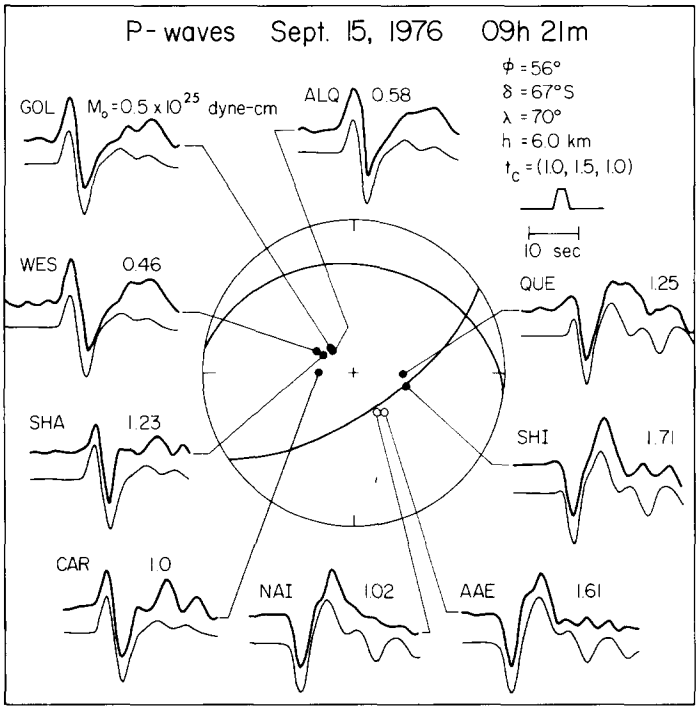

FIG. 10. Observed and synthetic *P* waves for the aftershock of 09h 21m, September 15, 1976. Synthetics are computed for a point source at 6-km depth in the Angenheister *et al.* (1972) structure (Table 4). Notation is the same as Figure 7.

stations are clearly reversed. An important observation was made by Ritsema (1976) on long-period vertical seismographs at de Bilt, the Netherlands. He observed a clear change in polarity between the main shock and 09h 21m aftershock on one hand and the 03h 15m shock on the other. Focal mechanisms for both aftershocks

are shown in Figure 9. No attempt was made to model the long-period body waves because of the noise present on the seismograms.

The mechanism of the 03h 15m aftershock appears to represent predominantly dip-slip fault motion, but with a considerable strike-slip component. In contrast to the other mechanism in which the nodal plane strike nearly east-west, the focal planes of this aftershock strike north and northeast. There are no major northeast-southwest striking structures in the area, although Martinis (1975; his Figure 13) does indicate several minor north-south trending lineations.

The mechanisms determined in this paper are somewhat different from mechanisms published for earlier earthquakes in the Friuli region. McKenzie (1972) suggests that the event of October 18, 1936 had a normal faulting mechanism, although Ahorner *et al.* (1972) present a strike-slip mechanism for this earthquake.

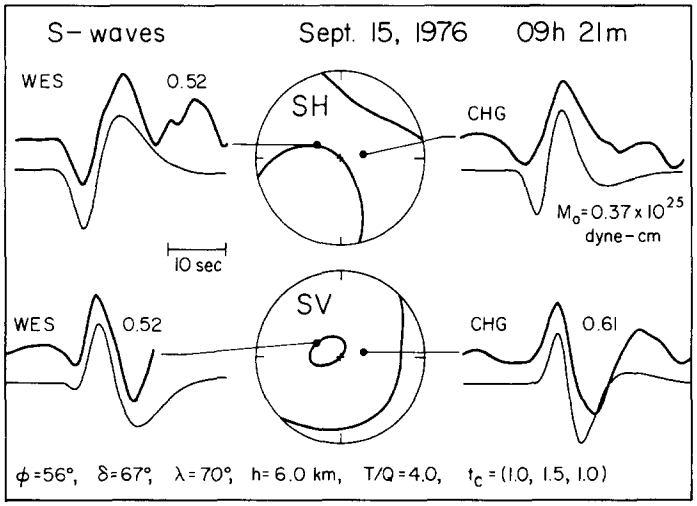

FIG. 11. *S* waves for the aftershock of 09h 21m showing observed and synthetic records and *SH* and *SV* radiation patterns.

Mayer-Rosa *et al.* (1976) studied the mechanism for the event of March 24, 1975 (m_b = 4.2, USGS). There is considerable ambiguity in the solution because the earthquake is quite small. The event is either strike-slip, or as Mayer-Rosa *et al.* prefer, thrust on an almost east-west striking fault plane.

FINITE FAULT

Up to this point, the body-wave records have been interpreted using synthetic seismograms computed for a point source in a layered half-space. Two assumptions are made in computing point source synthetics. The first is that the same time function is used for each ray (e.g., *P*, *pP*, *sP*, etc.), and the second is that the same time function is used for all azimuths and take-off angles. For an arbitrarily oriented, propagating shear fault, these assumptions are invalid. This is because *P* and *S* rays each require a different time function, and also, the time function observed at any point is dependent on the angle between the direction of rupture propagation and the take-off angle (Savage, 1966).

It is the purpose of this section to investigate the nature of fault propagation during the Friuli main shock using the formulation of Heaton (1978) which allows arbitrarily complex faulting histories. In the present discussion, we will try to place

constraints on the fault area and mode of rupture propagation, either unilateral or bilateral. To simplify the problem, it is assumed that the shallowly dipping nodal plane of Figure 4 is the fault plane, that the dislocation is uniform over the entire fault surface, and that the rupture velocity is 3.0 km/sec. Furthermore, the shape of the fault plane is a square, and the dislocation rise time is 1 sec. The six cases investigated are shown in Figure 12; the heavy broken line is the approximate limit of aftershock concentration from Figure 2, and the stars represent the epicenters as determined by various agencies. In the *upper* part of Figure 12, the square-fault planes are centered on the epicenter determined by Rome which is near the middle of the aftershock distribution. Three cases, fault lengths of 8, 16, and 24 km, are

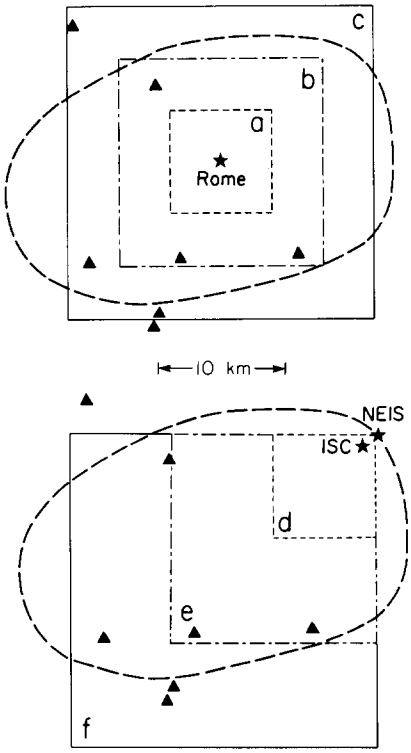

FIG. 12. Fault models used for the finite fault calculations. Six cases are shown corresponding to square faults of length 8, 16, and 24 km. In the *upper* part of the figure, the theoretical fault planes are centered on the epicenter determined by Rome which lies near the center of the aftershock distribution. The *lower* part shows the same fault planes, only now aligned so that the *upper* right corner (northeast) is near the NEIS and ISC epicenters. Dashed line indicating the limits of aftershock concentration gives a sense of scale.

computed. The superposition of the theoretical fault planes on the aftershock distribution is rather arbitrary, but it does give a sense of scale. The *lower* part of Figure 12 shows the case in which the fault originates at one corner of the fault plane and propagates unilaterally updip and toward the west. The NEIS and ISC epicenters are near the northeast (down-dip) corner of the aftershock distribution.

Synthetics for the six cases are shown in Figures 13 and 14. The model which best fits the P waves seems to be case c. The observed data do not change very much with azimuth. As expected, the symmetrically expanding cases (a, b, c) reproduce this effect quite well. This is in contrast to the unilateral faults, especially case f, which exhibit strong azimuthal variation. However, unilateral propagation cannot

be ruled out. For instance, case e fits the *P*-wave data almost as well as case c. What can be said instead is that there cannot be a strong propagation effect. Nor can the fault plane be substantially smaller than the aftershock area. Cases a and d give rise to synthetic seismograms which are much too narrow in duration compared to the

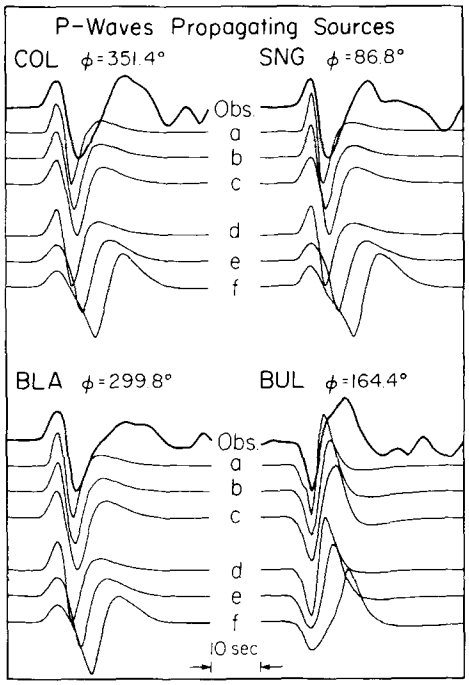

FIG. 13. Observed *P* waves of four stations compared to synthetics computed for finite fault models a through f.

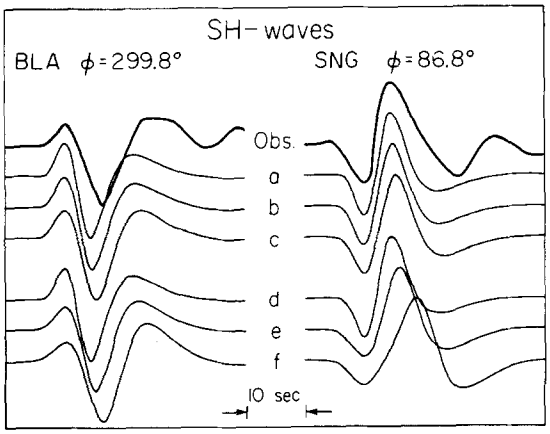

FIG. 14. Observed *SH* waves compared to synthetics computed for the finite fault models.

observed data. From these results, the probable fault length is 16 to 24 km, but whether faulting initiated at the center or edge of the zone cannot be determined.

Additional constraint on the rupture mechanism is provided by *SH* waves (Figure 14). Again, case f with strong azimuthal variation is ruled out by the data as are the cases with small fault planes (cases a, d). It must be kept in mind that the uncertainty in the value of attenuation for *SH* waves can have considerable effect on pulse width.

Rayleigh Wave Data

An independent estimate of the focal mechanism and seismic moment is provided by surface waves. In this study, the observed spectral density of 100-sec Rayleigh waves are compared to theoretical values calculated using the tables published by Ben Menahem *et al.* (1970). The observed data were prepared by first digitizing the seismogram in a group velocity window between 4.0 and 3.5 km/sec, then detrending and interpolating to a uniform time interval. The spectral density was obtained by a Fast Fourier transform program. The spectrum was corrected for instrument response according to the formulation of Hagiwara (1958) and normalized to a propagation distance of 90° using the equation

$$\sqrt{\frac{\sin\frac{\Delta}{a}}{\sin\frac{\Delta_0}{a}}}\exp[\gamma(\Delta-\Delta_0)]$$

where

Δ = epicentral distance

Δ_0 = normalized distance (= 90°)

a = Earth radius

γ = attenuation coefficient.

The attenuation coefficients of Ben Menahem *et al.* (1970) are used.

In Figure 15, the observed values of spectral density for 100-sec Rayleigh waves are compared to the theoretical radiation pattern computed for the source model found using body waves (strike = 76°, dip = 75°, rake = 80°, depth = 10 km). The

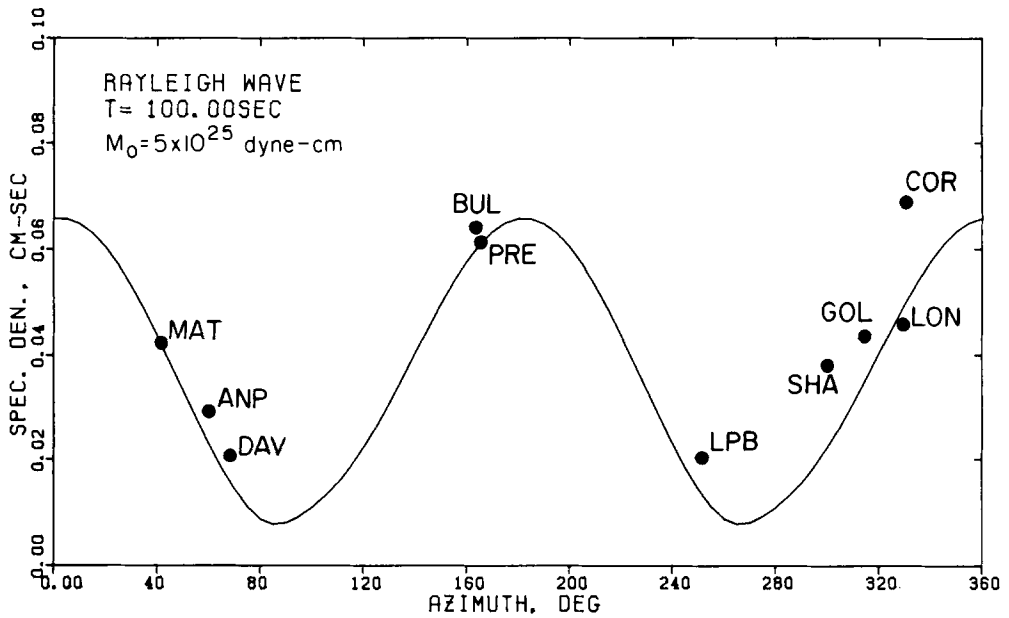

FIG. 15. Observed spectral density of 100-sec Rayleigh waves radiated by main shock compared to theoretical pattern for focal mechanism shown in Figure 4. Seismic moment is 5×10^{25} dyne-cm.

good agreement between the observed data and theoretical calculations indicate that the overall deformation recorded by 100-sec waves is the same as that recorded by ∿15-sec waves. However, the seismic moment determined from 100-sec surface waves is 5×10^{25} dyne-cm, somewhat higher than the value of 2.9×10^{25} dyne-cm found for body waves.

Discussion

A notable feature of the Friuli earthquake sequence is the large size of the September aftershocks relative to the main shock. The seismic moment of the September 15 (09h 21m) aftershock studied in this paper is nearly one-third the moment of the mainshock. Besides that earthquake, there were three other large events between September 11 and 15, 1976 (Table 1). To provide a quantitative measure of the energy release of the aftershock series, the seismic moment (M_0) can be estimated from local magnitude (M_L) using the relation $\log M_0 = 15 + 1.7 M_L$ (Wyss and Brune, 1968). The moment sum of the Friuli earthquake sequence from May 1976 through December 1977 is slightly over 8×10^{25} dyne-cm, of which $3 \times$

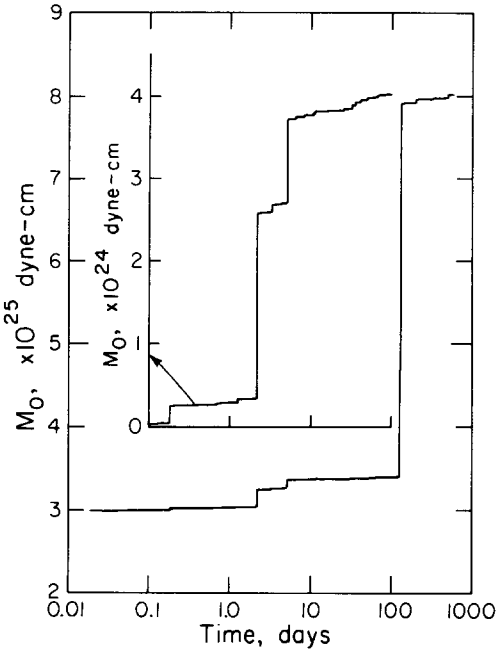

Fig. 16. Summation of seismic moment with time for earthquakes of the Friuli sequence calculated from an empirical relation between local magnitude and seismic moment.

10^{25} dyne-cm was released during the main shock (Figure 16). Thus, the aftershock sequence was considerably more energetic than the main shock. In contrast to the Friuli series, Hadley and Kanamori (1978) estimated the moment sum of the aftershocks of the 1971 San Fernando earthquake to be about 3.5×10^{24} dyne-cm, nearly two orders of magnitude smaller than the main shock. Also shown in Figure 16 is an enlargement of the energy-release curve for the first 100 days of aftershock activity. This curve is directly comparable to Figure 2 of Hadley and Kanamori (1978). Comparing the two diagrams, note that moment sum for Friuli sequence is somewhat larger than for San Fernando, and that most of the energy release came during two large earthquakes. It appears that the mechanical properties of the San

Fernando and Friuli seismic zones are rather different. In the case of San Fernando, most of the energy was released by a single, large earthquake. For Friuli, the seismic energy was liberated in a series of smaller earthquakes.

There are tantalizing hints of similar behavior during past earthquakes. For the earthquake of March 26, 1511, in particular, felt reports collected by Ambraseys (1976a, b) mention that the main shock was followed by a series of strong aftershocks, especially those of June 6 and August 8, 1511.

Finetti *et al.* (1979) have postulated a rather detailed history for the Friuli sequence involving various mapped tectonic structures. Given the uncertainty in depth and location of the earthquakes (Cagnetti and Console, 1977), it is premature to try to assign any one shock to any particular structure. It is reasonable to propose, however, that the main shock relieved the stress in one part of the fault zone and that the large September aftershock occurred in another part of the fault zone.

The historic earthquakes are not concentrated just in the Friuli region, but scatter over a wide area, about 200 km east to west (Ambraseys, 1976a). Ambraseys noted that activity seemed to alternate from one region to another over a period of several hundred years. Perhaps just as significant is that the events more or less span the width of the plate margin postulated by Lort (1971) and McKenzie (1972) (Figure 1). This is certainly not a subduction zone in the classical sense. More likely, this zone of seismicity is one of several areas of crustal shortening caused by the collision of Africa and Eurasia.

Knowing the seismic moment and fault area, the dislocation (D_0) and stress drop ($\Delta\sigma$) can be estimated for the main shock and aftershock. Using the formula for moment, $M_0 = \mu D_0 S = 4 \times 10^{25}$ dyne-cm where S is the fault area (about 20 km by 20 km), and μ is the rigidity ($= 3 \times 10^{11}$ dynes/cm^2), D_0 is calculated to be 33 cm for the main shock. For a circular fault, the stress drop is given by $\Delta\sigma = (7\pi/16)(\mu D_0/a)$ where a is the fault radius (Kanamori and Anderson, 1975). Using this formula, the stress drop is estimated to be 12 bars, with $a = 11.3$ km (the radius of a 400 km^2 circle) and the above value of D_0. These values of dislocation and stress drop are similar to those computed by Caputo (1976), using somewhat different methods.

For the aftershock, the fault area is about 10 km by 10 km from a comparison of observed records to finite fault models. Using the moment of 1×10^{25} dyne-cm, the dislocation is estimated to be 33 cm, with a stress drop of 24 bars. It is interesting to note that these stress drops are similar to stress drops of interplate earthquakes (Kanamori and Anderson, 1975) even though the plate margin here is not well defined.

Conclusions

In this paper have been presented source models for two earthquakes of the 1976 Friuli, Italy sequence: the main shock and aftershock of September 15 (09h 21m). The mechanisms of both earthquakes are similar. Regional geology and aftershock distribution suggests that the plane which dips gently to the north is the fault plane. This plane represents thrusting of the Alps over the sedimentary basin to the south. Both events occur at about 6- to 10-km depth and have moments of 3×10^{25} dyne-cm for the main shock and 1×10^{25} dyne-cm for the aftershock. No strong effects of fault propagation are present in the data suggesting either that the rupture began near the middle of the fault plane and expanded outward uniformly, or if the rupture began at one edge of the plane, the length of fault propagation was rather small. Synthetic seismogram calculations including the effect of source finiteness indicate that the fault length for the main shock is about 16 to 20 km. Using the above

values of seismic moment and fault area, the dislocation is estimated to be 33 cm and the stress drop 12 bars for the main shock. For the aftershock, these quantities are 33 km and 24 bars, respectively.

The large size of the aftershock series which began in September suggests that these events occurred in another part of the fault zone other than the main shock. Energy release during the Friuli earthquake sequence occurred in a main shock followed by several large aftershocks over the course of several months. In contrast, most of the energy released during the 1971 San Fernando, California earthquake was liberated by the main shock, with only a minor contribution from the aftershock sequence. The mechanism determined for the main shock is consistent with plate tectonic interpretations of Lort (1971) and McKenzie (1972).

Acknowledgments

The author wishes to thank John Ebel, Don Helmberger, Jim Pechmann, and Terry Wallace for critically reading the manuscript. Tom Heaton generously provided his program to compute finite fault synthetics. Laszlo Lenches and Joe Galvan drafted the figures.

This research was supported by the Advanced Research Projects Agency of the Department of Defense and was monitored by the Air Force Office of Scientific Research under Contract F49620-77-C-0022 and also by the Earth Sciences Section, National Science Foundation Grant EAR78-14786.

References

Ahorner, L., H. Murawski, and G. Schneider (1972). Seismotektonische traverse von der Nordsee bis zum Apennin, *Geol. Runds.* **61,** 915–942.

Amato, A., P. F. Barnaba, I. Finetti, G. Groppi, B. Martinis, and A. Muzzin (1976). Geodynamic outline and seismicity of Friuli-Venetia-Julia region, *Boll. Geof. Teor. Appl.* **18,** 217–256.

Ambraseys, N. N. (1976a). The Gemona di Friuli earthquake of 6 May 1976, in *The Gemona di Friuli Earthquake of 6 May 1976,* UNESCO Technical Report RP/1975-76/2.222.3, Paris, France.

Ambraseys, N. N. (1976b). Engineering seismology aspects of the Gemona-Friuli earthquake, *Boll. Geof. Teor. Appl.* **18,** 257–272.

Angenheister, G., H. Bögel, H. Gebrande, P. Giese, P. Schmidt-Thomé, and W. Zeil (1972). Recent investigations of surficial and deeper crustal structures of the Eastern and Southern Alps, *Geol. Runds.* **61,** 349–395.

Ben Menahem, A., M. Rosenman, and D. G. Harkrider (1970). Fast evaluation of source parameters from isolated surface-wave signals, *Bull. Seism. Soc. Am.* **60,** 1337–1387.

Burdick, L. J. and G. R. Mellman (1976). Inversion of the body waves from the Borrego Mountain earthquake to the source mechanism, *Bull. Seism. Soc. Am.* **66,** 1485–1499.

Cagnetti, V. and R. Console (1977). Space-time distribution of the Friuli (1976) earthquakes, *Ann. Geofis.* **30,** 107–184.

Caputo, M. (1976). The area of the fault, the dislocation, the stress drop and the seismic moment of the Friuli earthquake of May 6th, 1976, *Ann. Geofis.* **29,** 171–178.

Chung, W. Y. and H. Kanamori (1976). Source process and tectonic implications of the Spanish deep-focus earthquake of March 29, 1954, *Phys. Earth Planet. Interiors* **13,** 85–96.

Console, R. (1976). Meccanismo focale del terremoto del Friuli del 6 Maggio 1976, *Ann. Geofis.* **29,** 165–170.

Console, R. and C. Gasparini (1976). Hypocentral parameters for the Friuli, May 6th 1976 earthquake (in Italian), *Ann. Geofis.* **29,** 153–159.

Ebblin, C. (1976). Orientation of stresses and strains in the Piedmont area of eastern Friuli, NE Italy, *Boll. Geofis.* **18,** 559–579.

Finetti, I. and C. Morelli (1972). Deep seismic refraction exploration on Eastern Alps, *Bull. Geof. Teor. Appl.* **14,** 59–66.

Finetti, I., M. Russi, and D. Slejko (1979). The Friuli earthquake (1976–1977), *Tectonophysics* **53,** 261–272.

Futterman, W. I. (1962). Dispersive body waves, *J. Geophys. Res.* **67,** 5279–5291.

Gutenberg, B. and C. F. Richter (1954). *Seismicity of the Earth,* Hafner Publishing Company, New York, 310 pp.

Gwinner, M. P. (1971). *Geologie der Alpen,* Schweizerbart, Stuttgart, 477 pp.

Hadley, D. and H. Kanamori (1978). Recent seismicity in the San Fernando region and tectonics in the west-central Transverse Ranges, California, *Bull. Seism. Soc. Am.* **68,** 1449–1457.

Hagiwara, T. (1958). A note on the theory of the electromagnetic seismograph, *Bull. Earthquake Res. Inst., Tokyo Univ.* **36,** 139–164.

Haskell, N. A. (1962). Crustal reflection of plane *P* and *SV* waves, *J. Geophys. Res.* **67,** 4751–4767.

Heaton, T. H. (1978). *Ph.D. Thesis*, California Institute of Technology, Pasadena, California.

Helmberger, D. V. (1974). Generalized ray theory for shear dislocations, *Bull. Seism. Soc. Am.* **64,** 45–64.

Kanamori, H. and D. L. Anderson (1975). Theoretical basis of some empirical relations in seismology, *Bull. Seism. Soc. Am.* **65,** 1073–1095.

Karnik, V. (1971). *Seismicity of the European Area, Part II*, D. Reidel Publishing Company, Dordrecht-Holland, 218 pp.

Langston, C. A. and D. V. Helmberger (1975). A procedure for modeling shallow dislocation sources, *Geophys. J.* **42,** 117–130.

Lort, J. M. (1971). The tectonics of the eastern Mediterranean: a geophysical review, *Rev. Geophys. Space Phys.* **9,** 189–216.

Martinis, B. (1975). The Friulian and Julian Alps and Pre-Alps, Chapter 2 in *Structural Model of Italy*, L. Ogniben, M. Parotto, and A. Praturlon, Editors, Consiglio Nazionale delle Ricerche, Rome.

Mayer-Rosa, D., N. Pavoni, R. Graf, and B. Rast (1976). Investigations of intensities, aftershock statistics and the focal mechanism of Friuli earthquakes in 1975 and 1976, *Pure Appl. Geophys.* **114,** 1095–1103.

McKenzie, D. P. (1972). Active tectonics of the Mediterranean Region, *Geophys. J.* **30,** 109–185.

Müller, G. (1977). Fault-plane solution of the earthquake in northern Italy, 6 May 1976, and implications for the tectonics of the eastern Alps, *J. Geophys.* **42,** 343–349.

Papazachos, B. C. (1973). Distribution of seismic foci in the Mediterranean and surrounding area and its tectonic implications, *Geophys. J.* **33,** 421–430.

Ritsema, A. R. (1976). Preliminary analysis of Friuli earthquake records, *Boll. Geof. Teor. Appl.* **18,** 875–887.

Savage, J. C. (1966). Radiation from a realistic model of faulting, *Bull. Seism. Soc. Am.* **56,** 577–592.

Wyss, M. and J. N. Brune (1968). Seismic moment, stress and source dimensions for earthquakes in the California-Nevada region, *J. Geophys. Res.* **73,** 4681–4694.

SEISMOLOGICAL LABORATORY
DIVISION OF GEOLOGICAL AND PLANETARY SCIENCES
CALIFORNIA INSTITUTE OF TECHNOLOGY
PASADENA, CALIFORNIA 91125
CONTRIBUTION NO. 3320

Manuscript received November 15, 1979